Catalysis Today 171 (2011) 43–51

Contents lists available at ScienceDirect

Catalysis Today

journal homepage: www.elsevier.com/locate/cattod

Enhanced hydrogen production by in situ CO_2 removal on $CaCeZrO_x$ nanocrystals

Kazi Saima Sultana, De Chen*

Department of Chemical Engineering, Norwegian University of Science and Technology, Sem Sælands vei 4, NO-7491 Trondheim, Norway

ARTICLE INFO

Article history:
Received 31 October 2010
Received in revised form 7 April 2011
Accepted 8 April 2011
Available online 17 June 2011

Keywords:
CO_2 capture
Sorption capacity
Sorption enhanced
Steam reforming
Solid acceptors

ABSTRACT

The CO_2 capture properties of a new nanocrystalline CaO-based mixed oxide ($CaCeZrO_x$) were studied in both TGA and a fixed bed reactor. The kinetics of CO_2 capture at dry conditions was compared between these two reactors. The application of the new CO_2 acceptor in sorption enhanced steam methane reforming was studied by a fixed-bed reactor in the presence of 40 wt% nickel hydrotalcite catalysts. Experimental results show that the new CO_2 acceptor, $CaCeZrO_x$ has a significantly improved CO_2 capture capacity and cyclic reaction stability compared to natural dolomites, because of the large pores and stable backbone structure. It has also been observed that the sorption enhanced steam methane reforming in the fixed bed reactor produces more than 95% H_2 in a single-step process. Increase in production of hydrogen and higher CO_2 capture capacity are also observed with an increase in the residence time of methane. Steam has a significant effect on the stability of the acceptors, but not very much on the kinetics and capacity of CO_2 capture. The capacity of CO_2 capture on the acceptors in the SESMR process cannot be predicted by the independent CO_2 capture kinetic study on acceptor alone. A synergy effect between the sorption enhanced reactions and CO_2 capture on the CO_2 capture capacity was observed on the all solid CaO based CO_2 acceptors.

1. Introduction

Hydrogen is considered as a clean energy carrier for sustainable energy consumption. The most common industrial process for production of hydrogen from hydrocarbons is steam methane reforming (SMR). The hydrogen production from steam methane reforming process involves multiple steps and severe operating conditions. The reformer is normally operated at high temperatures and high pressures and large amount of energy is necessary to maintain the reaction temperature. An approach to improve SMR process is sorption enhanced reaction process (SERP) for hydrogen production, which combines the reforming and water–gas shift reactions with in situ removal of the produced CO_2 by means of adsorption or the carbonation reaction [1–3]. Such a configuration has a number of technologically beneficial consequences: it provides a favourable shift in thermodynamic equilibrium toward hydrogen production, decreases the reaction temperature and removes carbon dioxide from the hydrogen product stream, thus decreasing the requirements for hydrogen purification. All these steps reduce the investment and operation cost of sorption enhanced steam methane reforming (SESMR). However, the performance of SESMR depends on the selection of appropriate CO_2 acceptor. A detailed study of the properties of CO_2 acceptors under real steam reforming conditions is very appreciated for a better understanding of the SERP.

Several solid CO_2 acceptors such as Li_2ZrO_3 [4,5], Na_2ZrO_3 [6] and CaO mixed oxides [7] have been tested for high temperature CO_2 capture. A process evaluation revealed that the CaO is the best acceptor due to its proper thermodynamic properties for hydrogen production by SESMR [4]. The properties of CaO based CO_2 acceptors including the CO_2 sorption capacity and durability at different operation conditions and their applications in sorption enhanced steam methane reforming has been demonstrated and intensively studied [2,8–10]. For example, Han and Harrison [2] used CaO to capture CO_2, overcoming the equilibrium limitation and achieving complete CO conversion. Dolomite was used as precursor and the combined water gas shift and carbonation reactions were studied in a laboratory-scale fixed bed reactor. Balasubramanian et al. [11] added a calcium based CO_2-acceptor to a commercial nickel-catalyst producing >95% H_2 in a laboratory-scale fixed bed reactor in the temperature range of 723–1023 K in SESMR. Yi and Harrison [12] used uncalcined dolomite admixed with commercial catalyst to produce 92% H_2 at the low temperature of 733 K at a steam to methane ratio to 3. Recently CaO nanocrystals doped with different oxides have been drawn increasing attention due to the high capacity and improved properties [13–15]. A wide range of CaO mixed with Si, Ti, Cr, Co, Zr and Ce oxides were tested and Ca–Zr–O mixed oxides was found to exhibit the best performance [13]. Li et al. used $CaO–Ca_{12}Al_{14}O_{33}$ and succeeded at constant capacity of 5 ml/kg for 13 cycles [16]. The stable performance of the material

* Corresponding author.
E-mail address: chen@chemeng.ntnu.no (D. Chen).

0920-5861/$ – see front matter © 2011 Elsevier B.V. All rights reserved.
doi:10.1016/j.cattod.2011.04.019

was attributed to the presence of $Ca_{12}Al_{14}O_{33}$. During our development of new CO_2 acceptors, formation of pervoskite $CaZrO_3$ and spinel structure $CaAl_2O_4$ oxide was found to reduce CO_2 capture capacity. Here we report new calcium based mixed oxide; namely, $CaCeZrO_x$ where the formation of pervoskite structure of Ca–Zr is suppressed, thus a high CO_2 capture capacity is achieved.

Capture of CO_2 by CaO acceptors is based on the reversible reactions between CaO and CO_2, leading to the formation of $CaCO_3$ as follows:

$$CaO + CO_2 \leftrightarrow CaCO_3$$

Steam has been recognized to influence the above carbonation reactions of the calcium based acceptors. The effect of steam on the carbonation on CaO, dolomite was addressed by several authors [17–20]. Carbonation properties of the Ca based acceptors can be changed by the addition of steam. Addition of steam was reported to enhance carbonation rate of the CaO–CO_2 reaction of calcined dolomite [21], but such enhancement was not further confirmed in another study [17]. Zeman studied the effect of steam hydration on the performance of lime as acceptor for CO_2 capture. He concluded that hydration leads to improve stability of CaO, but their results do not give conclusive evidence on the effect of hydration on the kinetics. Han et al. [22] found that addition of steam to the CO_2/N_2 mixture had a little effect on the ultimate capacity of CaO acceptors. Manovic and Anthony [18] also observed similar effect of steam concentration (10% and 20% H_2O) on carbonation of limestone (Kelly Rock) at 773 K and 873 K. They found that steam concentration in this range does not significantly affect the conversion profiles. No influence of steam concentration was observed at 873 K, and only a small enhancement was observed at 773 K at higher steam concentration. Steam has been reported having benefits on cyclic stability of limestone when cyclic carbonation was conducted at a mild temperature of 573 K. On the contrary, opposite effect of steam was observed under SESR relevant conditions [1]. A detailed kinetic study on a well-defined structure of CaO based acceptor is appreciated to gain better understanding of steam effects on carbonation reaction.

Thermogravimetric analysis (TGA), fixed bed reactor and tapered element oscillating microbalance (TEOM) reactor have been applied for experimental evaluation of acceptors for CO_2 capture and regeneration. There are several advantages and disadvantages of these methods. Among them TGA is the most commonly used technique for measuring the weight change of acceptors during the periods of carbonation and decarbonation. Several workers have investigated the multi-cycle performance of CaO-based acceptors mostly by TGA [11,16,22]. However, due to the oven limitation of some TGA, it is difficult to use TGA to conduct a high temperature measurement with gas flow containing steam at a well-defined partial pressure. In addition, a large bypass in the conventional TGA could limit its application in kinetic study [23,24]. Also a TEOM has been used for the evaluation of CO_2 capture properties in presence of steam [25]. But the difficult operation and low availability of the TEOM make it inconvenient in some cases. Fixed bed reactor can be used for operating the carbonation/decarbonation reactions with acceptors. It is also possible to conduct experiment in presence of steam at different conditions. Compared to TGA, a fixed bed reactor has well controlled contact between all the gas and solid acceptors [26]. As a result, tests on the acceptor in a fixed-bed reactor could provide more reliable kinetic information.

In this paper, we have synthesized the new $CaCeZrO_x$ mixed oxide acceptor and evaluated its kinetic performance of CO_2 capture and regeneration as well as stability in the absence and presence of steam using TGA and the fixed bed reactor at relevant SESMR conditions. Kinetics of carbonation and decarbonation of CaO based acceptors were compared between using TGA and fixed bed reactors. This paper also reports steam reforming experimental results from a laboratory-scale fixed bed reactor loaded with nickel-hydrotalcite (Ni-HTlc) catalysts and synthetic $CaCeZrO_x$ acceptors. The CO_2 capture capacity and stability measured at the reaction conditions of SESMR are compared to one in CO_2 capture kinetic studies. A synergetic effect between sorption enhanced reforming and in situ CO_2 capture on the CO_2 capture capacity is identified. The effect of the methane space velocity on hydrogen production and CO_2 removal is also addressed.

2. Experimental

2.1. Preparation of $CaCeZrO_x$ acceptor

Calcium based mixed oxide $CaCeZrO_x$ was prepared [27] by mixing calcium acetate (Fluka), cerium nitrate (Fluka) and zirconium nitrate (Fluka) precursors at a molar ratio 10:1:1. The precursors were dissolved in deionized water and the solution was stirred for one day to form slurry. The slurry was then spray-dried at 473 K using a spray dryer (*Buchi, Mini Spray drier, B-191*) to produce micro-sphere acceptors with an average particle size ranging between 40 and 100 nm. The following parameters of the spray dryer were kept constant during experiment: drying temperature 273 K, pump speed 10 rpm corresponding 8.1 cm^3/min of the solution of mixed oxides precursors and fan speed of 50 corresponding to 4.3 m/s of air. After spray drying the material was calcined in a calcination oven at 1023 K (3 K/min) in air for 3 h and a nominal ratio of CaO, CeO_2 and ZrO_2 was estimated based on the precursor materials.

2.2. Preparation of Ni-HTlc catalyst

A Ni–Mg–Al hydrotalcite-like catalyst was prepared by coprecipitation method of Mg $(NO_3)_2{\cdot}6H_2O$, Al $(NO_3)_3{\cdot}9H_2O$ and Ni $(NO_3)_2{\cdot}6H_2O$ to obtain 40 wt% Ni (40Ni-HTlc) The atomic ratio, $x = M^{2+}/M^{2+} + M^{3+}$ is fixed at 0.25. The Ni-HTlc catalyst was prepared following the procedure mentioned previously [28,29]. After preparation, the catalyst was dried over night under vacuum at 343 K and calcined at 873 K for 6 h flowing air using a heating rate of 5 K/min.

The selected properties of the catalyst and $CaCeZrO_x$ acceptor are summarized in Table 1.

2.3. Kinetic study in TGA and fixed bed reactor

Kinetic experiments were conducted in a thermogravimetric analyzer (Netzsch-STA 449). A small quantity (5.5–5.6 mg) of the material was placed in an alumina sample cup was initially heated at 1173 K, in the presence of 100 cm^3/min pure Ar to remove possible humidity and CO_2 adsorbed. The carbonation reaction was studied in the thermogravimetric analyzer at the CO_2 pressure range (0.1–0.8 bar) with a feed gas containing CO_2 and with the balance made up of an inert gas (Ar). The instrument records the increase in the sample weight with respect to time, which signifies the CO_2 capture by the acceptor.

TGA was used for multicycle test to perform the durability of the acceptor. The temperature programmed range was from 473 K to 1173 K. The heating rate was set to 10 K/min and the cooling rate was 50 K/min. The carbonation and regeneration measurements were used to describe the capacity of the acceptor, defined according to Eq. (1). The capacity is expressed in term of grams of CO_2 per gram of calcined acceptor.

$$\text{Capacity}\,(\%) = \left[\frac{\text{g of } CO_2}{\text{g of calcined acceptor}}\right] \times 100 \quad (1)$$

Table 1
Properties of $CaCeZrO_x$ and NiHTlc catalyst.

Reforming catalyst							Sorbent		
Ni-HTlc prepared by coprecipitation ~40 wt% Ni Ni:Mg:Al = l.33:1.66:1				$CaCeZrO_x$ prepared by spray drying $CaO:CeO_2:ZrO_2$ = 10:l:l			Arctic dolomite CaO (32%), MgO (20.3%), SiO_2 (0.7%), Al_2O_3 (0.1%), Fe_2O_3 (0.1%), Na_2O (0.003%), TiO_2 (0.0055%), K_2O (0.004%)		
BET surface area [m^2/g]	Ni dispersion [%]	d_{Ni}[a] [nm]	d_{NiO}[b] [nm]	BET surface area [m^2/g]	Pore volume (cm^3/g)	Crystal size (CaO) [nm]	BET surface area [m^2/g]	Pore volume (cm^3/g)	Crystal size [nm]
153.4	12.0	8.4	4	31.1	0.14	39	8.0	0.04	–

[a] Calculated from H_2 chemisorption.
[b] Calculated from X-ray diffraction.

During kinetic measurements in TGA and a fixed bed reactor, the internal and external mass transfer and heat transport limitations were excluded. External and internal mass transfer limitations were tested through the variation of the CO_2 flow (from 10 cm^3/min to 80 cm^3/min), inert gas and acceptor particle sizes (150–250 μm and 250–500 μm respectively). The acceptor particle sizes of 250–500 μm were found internal transport limitation free in the kinetic study at all the conditions studied into the present work, which were used in the rest of the kinetic studies. The CO_2 flow has been studied at different CO_2 pressures. For the most studied CO_2 pressures of 0.5 and 0.1 bar, 60 cm^3/min and 10 cm^3/min are found to be necessary to eliminate the external transport limitation in the fixed bed reactor.

CO_2 carbonation and regeneration experiments were carried out in a fixed bed reactor, namely a stainless steel reactor of 1 cm diameter. A small amount of acceptor (0.2190–0.2195 g) of particle size 250–500 μm and alumina wool were installed on the reactor to support the solid acceptors in the reactor. The reactor was placed into a furnace equipped with a temperature controller. Carbonation experiments were carried out with a gas mixture containing different amounts of CO_2, steam in nitrogen. CO_2 sorption experiments were carried out at 843 K. Online chemical analysis of CO_2, N_2 at the exit of the reactor was achieved by a gas chromatograph (Agilent 3000). N_2 was used as the internal standard.

The following Eq. (2) was used to calculate the capacity of $CaCeZrO_x$ [30]:

$$N_{CO_2} = \int_0^{t_1} (F_{CO_2,tot} - F_{CO_2,t})\,dt \quad (2)$$

Here, $F_{CO_2,tot}$ indicates the average value of CO_2 flow rate during saturation; $F_{CO_2,t}$ represents the CO_2 flow rate at time t; t_1 represents the time point where the CO_2 content in the gas effluent did not increase at all.

Regeneration experiments were also carried out in the same fixed bed reactor. Regeneration experiments were conducted to determine how effectively the acceptor could be regenerated. In order to study the effect of temperature on the activity of the regenerated acceptors, regeneration was achieved at three different temperatures, such as at 973 K, 1023 K and 1043 K. In order to proceed with the regeneration of the acceptor, the temperature of the reactor was increased from the capture temperature (843 K) to the regeneration temperatures, with a heating rate of 3 K/min. To avoid the possible decarbonation, a mixture of (80 cm^3/min CO_2/10 cm^3/min N_2) was used during heating until the corresponding regeneration temperature was achieved. When the required regeneration temperature was reached, the reaction atmosphere was changed from the gas mixture (80 cm^3/min CO_2/10 cm^3/min N_2) to 100 cm^3/min N_2. Regeneration experiments were continued until the concentration of CO_2 in the off-gas approached to zero.

2.4. Sorption experiment in fixed bed

Sorption enhanced steam reforming of methane was carried out in a stainless-steel fixed bed reactor with inner diameter of approximately 16 mm. The reforming catalyst was a Ni-based catalyst, Ni-HTlc (~40 wt% Ni), and $CaCeZrO_x$ was chosen as the acceptor. Both the catalyst and acceptor were crushed into powders with particle sizes in the range of 250−500 μm and installed into the reactor. Prior to the SESMR experiment, the calcined catalyst was reduced at 943 K (heating rate 3 K/min) for 10 h in a mixed flow of H_2 (50 cm^3/min) and Ar (50 cm^3/min). After the reduction, the temperature was decreased to 843 K. The reactor was flushed with Ar so that no H_2 was remaining in the reactor and after that the reactive gases were introduced in the reactor. The SESMR is divided into two sessions; the first session is steam reforming with in situ CO_2 capture following acceptor regeneration.

The flow rates of gases were controlled using Bronkhorst mass flow controllers (MFCs). Water at given steam to carbon ratio was fed by a Bronkhorst liquid flow controller swept by Ar flow, evaporated in a vaporizer and then directed into the reactor. SESMR was carried out at 843 K with steam to carbon ratio 3. The SESMR continued until the breakthrough of CO_2 content occurred. In the next session, the acceptor was thermally regenerated at 973 K for 1 h with a ramp rate of 2 K/min. Ar flow of 50 cm^3/min was used to sweep the released CO_2 and, at the same time, H_2 flow of 20 cm^3/min was fed to keep the Ni in metal state. Afterwards, the temperature of the reactor was regulated for a new SESMR reaction. The SESMR and regeneration session were repeated for several cycles to investigate the stability of the acceptor under cyclic conditions. Ar flow of 100 cm^3/min was used to flush the reaction system before a new session started. By separating steam using a condenser the product gas containing H_2, CO_2, CO and CH_4 entered for the GC for analysis.

The operating conditions for cyclic stepwise sorption-enhanced steam methane reforming (SESMR) and acceptor regeneration reactions over $CaCeZrO_x$ and Ni-HTlc catalyst are summarized in Table 2.

3. Results

Fig. 1 shows the CO_2 uptake curves obtained from both TGA and fixed bed reactor at temperature 843 K and two different partial pressures (0.1 bar and 0.5 bar). The CO_2 uptake capacity of $CaCeZrO_x$ estimated from the breakthrough curves of CO_2 at different CO_2 pressures (from 0.07 to 0.8 bar) and at 843 K on $CaCeZrO_x$ (Fig. 2) obtained from the fixed bed. The CO_2 uptakes are expressed in terms of mass of CO_2/mass of $CaCeZrO_x$, where the weight of the CaO based mixed oxide was measured by decarbonation of the sample in TGA.

The CO_2 capture capacities at different CO_2 partial pressures but at the constant temperature of 843 K obtained from both the fixed bed reactor and TGA are plotted together in Fig. 3. TGA and fixed bed

Table 2
Reaction conditions for SESMR.

Temp.	Pressure	Sorption			Regeneration		
		Gas composition	Gas flow rate	Temp.	Pressure	Gas composition	Gas flow rate
843 K	1 bar	90 mol% CH_4 10% N_2	100 cm^3/min	973 K	1 bar	100% Ar	100 cm^3/min

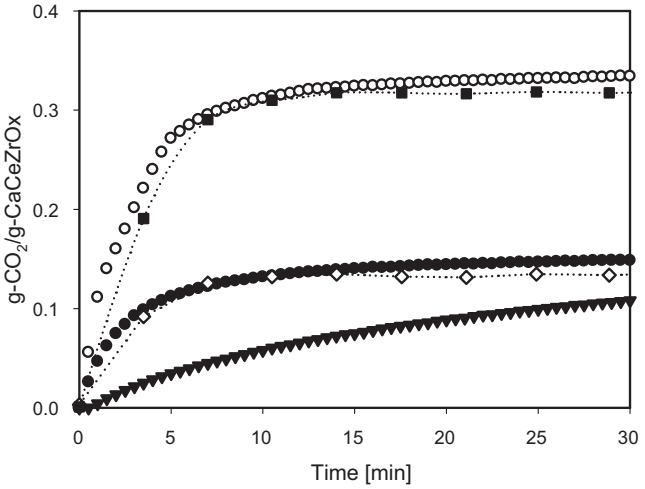

Fig. 1. Comparison of CO_2 uptake curve in TGA ($CaCeZrO_x$ = 5.5 mg, ● P_{CO_2} = 0.1 bar, F_{CO_2} = 10 cm^3/min, ▶ F_{CO_2} = 0.1 bar, F_{CO_2} = 20 cm^3/min, T = 843 K, Ar balance). Fixed bed ($CaCeZrO_x$ = 0.2190 g, ◊ P_{CO_2} = 0.1 bar; F_{CO_2} = 10 cm^3/min, ○ P_{CO_2} = 0.5 bar, F_{CO_2} = 50 cm^3/min, T = 843 K, N_2 balance).

reactor provide similar CO_2 capacity which increases concurrently with increasing CO_2 pressure.

Carbonation characteristics of the $CaCeZrO_x$ studied by fixed bed at different temperatures (783 K, 803 K, 843 K and 873 K respectively) are shown in Fig. 4. The carbonation rate increases with increasing temperature, but the capacity of CO_2 capture is independent of temperature.

CO_2 sorption experiments were carried out at 843 K in the presence of different steam concentrations (10% H_2O, 20% H_2O and 40% H_2O). The gaseous mixtures at the inlet of the reactor consist of three components such as CO_2, N_2, and steam. Fig. 5 shows the CO_2 uptake profiles over $CaCeZrO_x$ at several steam pressures. There is a weak effect of steam on carbonation rate observed.

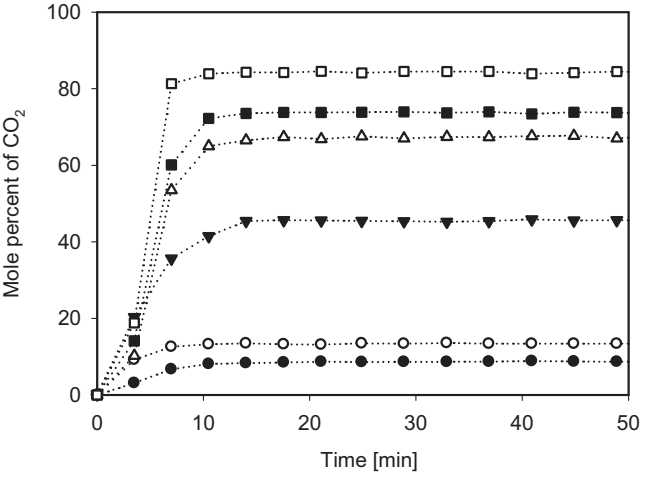

Fig. 2. CO_2 breakthrough curves in the fixed bed (acceptor: $CaCeZrO_x$ = 0.2190 g, CO_2 partial pressures: ● P_{CO_2} = 0.07 bar, F_{CO_2} = 7 cm^3/min, ○ P_{CO_2} = 0.1 bar, F_{CO_2} = 10 cm^3/min, ▼ P_{CO_2} = 0.5 bar, F_{CO_2} = 80 cm^3/min, Δ P_{CO_2} = 0.6 bar, F_{CO_2} = 60 cm^3/min, ■ P_{CO_2} = 0.7 bar, F_{CO_2} = 70 cm^3/min, and □ P_{CO_2} = 0.8 bar, F_{CO_2} = 80 cm^3/min, T = 843 K, N_2 balance).

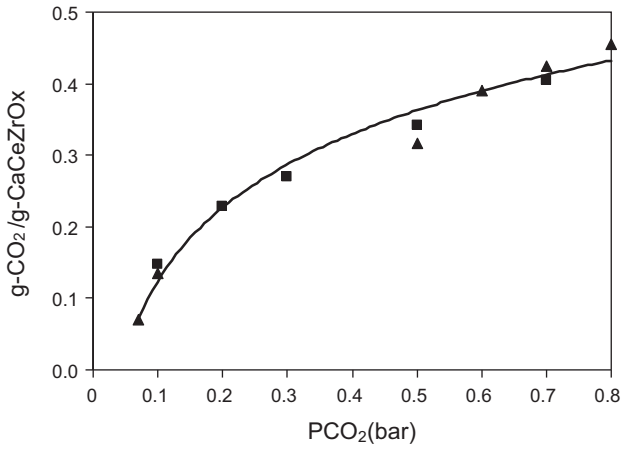

Fig. 3. CO_2 capture capacities of $CaCeZrO_x$ at different P_{CO_2} (T = 843 K, N_2 balance). ■ TGA ($CaCeZrO_x$ = 5.5 mg) and ▲ fixed bed reactor ($CaCeZrO_x$ = 0.2190 g).

Fig. 6 shows the effect of decarbonation of the acceptor. The decarbonation rate increases with increasing temperature. At all the three temperatures (973 K, 1023 K and 1043 K), $CaCeZrO_x$ can be completely regenerated when a temperature swing with N_2 flusing was used for decarbonation of the acceptor.

Regeneration of $CaCeZrO_x$ was performed at 973 K under inert atmosphere and a different amount of steam (10%, 40% and 70% H_2O) at 973 K is shown in Fig. 7. The gaseous mixtures at the inlet of the reactor consist of three components such as CO_2, N_2, and steam. Results show that steam promotes the decarbonation of the acceptor.

Typical reactor response from a fixed bed reactor for SESMR is shown in Fig. 8. Typically, the evolution of the gas effluent compositions in the SESMR reaction process takes place in three stages: pre-breakthrough, breakthrough, and post-breakthrough.

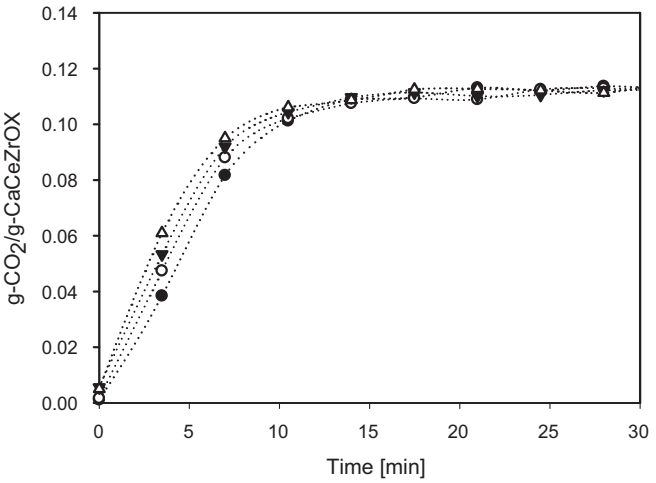

Fig. 4. CO_2 sorption uptake curves of $CaCeZrO_x$ at different temperatures: ● 783 K, ○ 803 K, ▼ 843 K and Δ 873 K ($CaCeZrO_x$ = 0.2195 g, P_{CO_2} = 0.1 bar, F_{CO_2} = 25 cm^3/min, N_2 balance).

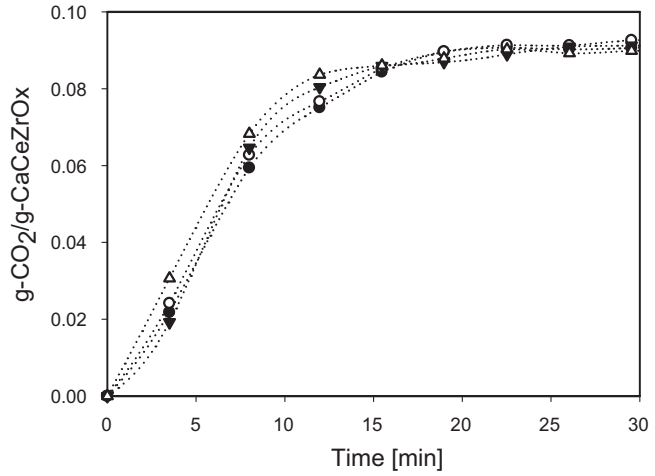

Fig. 5. CO_2 uptake curves at different amounts of steam ($CaCeZrO_x$ = 0.2190 g, P_{CO_2} = 0.07 bar, F_{CO_2} = 7 cm^3/min. ● No H_2O, ○ 10% H_2O, F_{H_2O} = 2.78 g/h, ▼ 40% H_2O, F_{H_2O} = 11.24 g/h, Δ 70% H_2O, F_{H_2O} = 19.69 g/h, T = 843 K, N_2 balance).

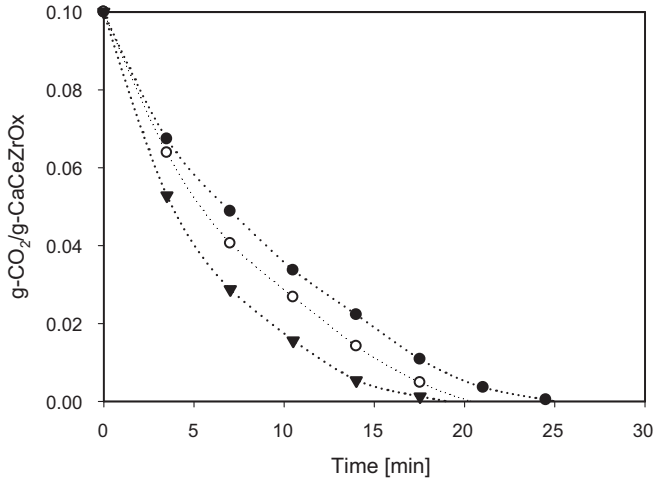

Fig. 6. Regeneration at different temperatures (● 973 K, ○ 1023 K, ◄ 1043 K) ($CaCeZrO_x$ = 0.2190, F_{N_2} = 100 cm^3/min).

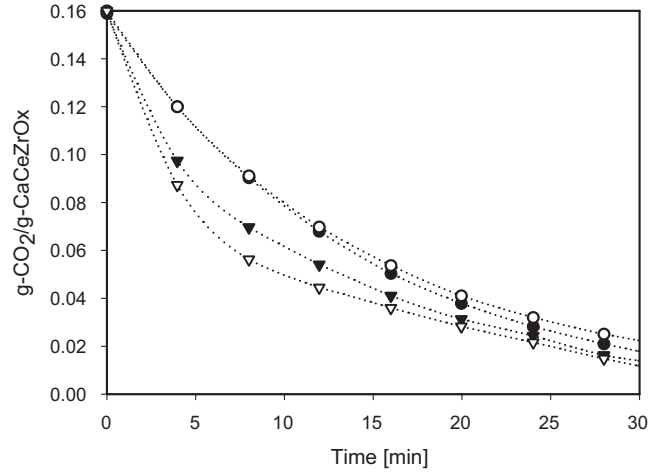

Fig. 7. Regeneration of $CaCeZrO_x$ acceptor at 973 K in dry and wet conditions: ○ no H_2O, ● 10% H_2O, F_{H_2O} = 2.78 g/h, ◄ 40% H_2O, F_{H_2O} = 11.24 g/h, Δ 70% H_2O, F_{H_2O} = 19.69 g/h ($CaCeZrO_x$ = 0.2190 g, F_{tot} = 100 cm^3/min, N_2 balance).

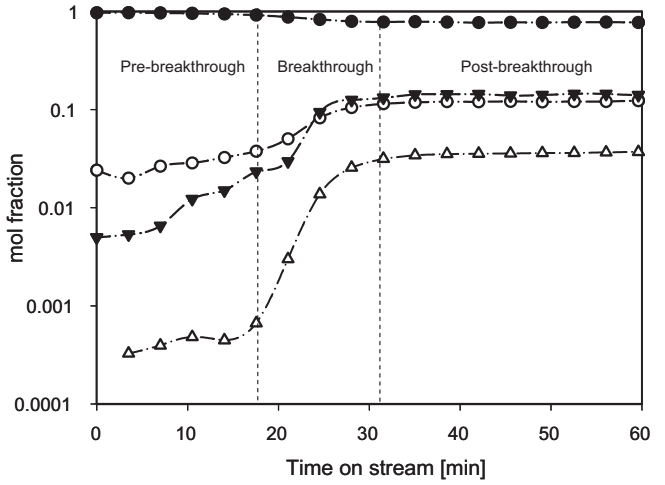

Fig. 8. Effluent H_2 and CO_2 concentration profiles on a dry basis (● H_2, ○ CH_4, ► CO_2, Δ CO). Acceptor: 5 g $CaCeZrO_x$, catalyst: 1 g 40 wt% NiHTlc. Acceptor/catalyst: 5, S/C: 3, F_{CH_4} = 45 cm^3/min, T: 843 K and P: 1 bar. Regeneration: T: 973 K, F_{Ar} = 100 cm^3/min.

Concentrations of H_2, CH_4, CO, CO_2 (dry basis) in the product gas are shown as a function of time (Fig. 8). As the SESMR reaction preceded, the reaction between CaO of the acceptor and CO_2 approached the second reaction regime, breakthrough period. The breakthrough represents the process approaching saturation of the CO_2 acceptors. At the second stage, CO_2 removal becomes less effective, and as a result CO conversion in the water gas shift reaction is limited. As seen in Fig. 8, during the stage of breakthrough, the CO_2 content increases rapidly. Decrease in the pre-breakthrough time and increase of the breakthrough time with increasing the carbonation–decarbonation cycle number implies acceptor deactivation. After breakthrough period, postbreakthrough period begins when the acceptor is exhausted and carbonation reaction rate approaches zero. In this stage, only the reforming and water gas shift reactions are active.

SESMR result in Fig. 8, a hydrogen yield 96.7% demonstrates the enhancing effect of the acceptor on the conversion of methane. A very low CO content (about 0.04%) was achieved at 843 K. It is expected to be further lower at the lower temperature based on thermodynamic analysis. As the acceptor started saturating, the hydrogen concentration decreased, whereas CO and CO_2 increased, finally equilibrating to values almost equal to those of SMR (about 76%).

4. Discussion

4.1. Comparative study of carbonation of $CaCeZrO_x$ in TGA and fixed bed

TGA have widely been used for the studies of carbonation and decarbonation of CO_2 acceptors. However, the flow of the CO_2 containing gas to the sample bed is not well defined in TGA, due to a bypass which often causes a problem in kinetic study [23,24]. Here we present a comparative study of kinetic study using both TGA and a fixed bed reactor to determine the feasibility and the limitation of the two different techniques.

The uptake curves in Fig. 1 measured by TGA and fixed bed reactor, clearly indicates that carbonation takes place in two stages. The first stage is very rapid, while the second stage is slow. CO_2 partial pressure has an important effect on the first stage of the carbonation kinetics. During the first stage of carbonation, reaction takes place between CaO as the active part of $CaCeZrO_x$ and CO_2 leading to the formation of surface $CaCO_3$. This part of the process is

reaction controlled [31]. The second stage of carbonation is rather slow and is diffusion-controlled, is almost linear with time. During the slow reaction regime, the reaction rate decreased because CO_2 need to diffuse through the formed $CaCO_3$ layer to reach the unreacted CaO. The surface of acceptor is covered and small pores are blocked by the formation of a nonporous carbonate product layer. This layer significantly hinders the inward diffusion of CO_2 [32].

It has been observed from Fig. 1 that the kinetic uptake in the fixed bed reactor is similar to TGA for two different partial pressures, in case that CO_2 flow is sufficiently high to eliminating external transport limitation. It is in contrast to the previously reported limitation of TGA in kinetic studies [23,24]. This is most likely that the carbonation rate of the CO_2 acceptor is relatively low. On the other hand, it indicates that TGA can be used for kinetic study of carbonation reaction of CaO based acceptors. It is also observed from Fig. 1 that the kinetic uptake is much faster in the fixed bed reactor than in the TGA when CO_2 flow is lower than 20 cm^3/min. This is due to the external diffusion limitation at low CO_2 flow. The flow rate should be much higher than in the fixed bed due to the bypass problem in the TGA in order to eliminate external transport limitation, especially for the low CO_2 pressure range.

Fig. 1 shows a deviation on the uptake in the second stage between the two techniques. It is mostly caused by a relatively low sensitivity of the GC analysis. A small change in the CO_2 concentration at the reactor exit due to a low reaction rate of the carbonation is difficult to be accurately detected. However, for the practical application only the fast stage of CO_2 uptake, which takes place for minutes, is of interest. CO_2 breakthrough curves (Fig. 2) show that as soon as the reactant gas is introduced into the fixed bed, CO_2 sorption onto the acceptor took place and saturation of the acceptor is reached in all cases within about 10 min.

Fig. 3 shows that the fixed bed and TGA show very similar capture capacity at each CO_2 pressure. The results in Fig. 3 show an increase in capture capacity of the new synthetic $CaCeZrO_x$ acceptor with increasing partial pressure of CO_2. Several investigators [16,33,34] have also observed a marked increase in uptake of CO_2 of synthetic mixed oxide acceptor with increase in pressure whereas the uptake of CO_2 natural acceptors is independent of partial pressure of CO_2 [33,35–38]. This increase in capacity with increasing CO_2 pressure suggests a $CaCO_3$ product layer in the nanocrystals. The CaO core is the domain of the carbonation reaction. CO_2 partial pressure is the key kinetic factor which influences the diffusion of CO_2 in gas–solid reaction zone, thus the thickness of the product zone, determining the CO_2 capture capacity of the $CaCeZrO_x$.

It has been reported that the molar volume of CaO increased from 16.9 cm^3/g of CaO to 36.9 cm^3/g of $CaCO_3$ during carbonation [39]. Carbonation of CaO inside the pores generates a $CaCO_3$ layer, reducing significantly the pore volume [40]. It caused significant CO_2 diffusion limitation in the $CaCO_3$ layer, thus limited the utilization of inner core of CaO. Results (Fig. 3) clearly suggest that the thickness of $CaCO_3$ layer depends on the CO_2 pressure and a high CO_2 pressure results in a thick product layer. A high CO_2 pressure obviously enlarges the CO_2 driving force for diffusion, enabling a deep penetration into the CaO crystals during the reaction–diffusion process.

4.2. Kinetic performance of carbonation and decarbonation of $CaCeZrO_x$

The uptake curves in Fig. 4 indicate a concurrent increase in the carbonation rate with increasing temperature, while the capacity is almost constant at the corresponding CO_2 pressure, regardless of the temperature. The $CaCeZrO_x$ nanocrystals can be saturated within about 10 min at the temperatures larger than 843 K and 0.1 bar CO_2. Both the CO_2 diffusion rate and the surface carbonation rate increase with temperature. But the temperature seems to have a very weak influence on the ratio of the CO_2 diffusion rate and the carbonation rate. Therefore temperature did not change the product layer thickness. It is in contrast to Li's observation [41] where the temperature increased significantly the product layer thickness, thus the CO_2 capture capacity of limestone. The difference could be caused by the crystal size and the surface composition.

Regeneration experiments were carried out at three different temperatures (973 K, 1023 K and 1043 K) respectively. Fig. 6 shows that $CaCeZrO_x$ acceptor is regenerated completely at these three temperatures and the rate of regeneration increases with increase in the temperature. This is due to the acceleration of decomposition rate of $CaCO_3$ with increasing temperature.

4.3. Steam effect on carbonation/decarbonation

In agree with the observation in literature [17–19,21,22,25] steam has a positive impact on the capture kinetics of CaO-based acceptors. Comparing to the literature observations, Fig. 5 shows that increasing steam concentration does not significantly affect CO_2 uptake profiles of the acceptor. Only a small increase in the carbonation rate is observed but not the capacity. This is consistent with the findings of Han et al. [22] in their multiple-cycle studies. But it is in contrast to the observation of Monovic et al. [18] where a enhanced CO_2 capture capacity of limestone by adding steam due to a enhanced diffusion in the product layer [18]. Fig. 7 shows a larger influence of steam on the decarbonation rate of $CaCeZrO_x$ acceptor comparing to the carbonation rate.

There are two reported possible mechanisms [42] for the reason of the enhancement of carbonation reaction. One of the proposed mechanisms in the CaO–$CaCO_3$ inner surface is shown as follows:

$$CO_2(g) \leftrightarrow CO_{2(ads)} \quad (3)$$

$$CO_{2(ads)} + O^{2-} \rightarrow {CO_3}^{2-} + \tfrac{1}{2}O_2 \quad (4)$$

$$CO_3^{2-} + CaO \rightarrow CaCO_3 + O^{2-} \quad (5)$$

O^{2-} released from steam can accelerate carbonation.

Another possible mechanism was pointed out that the steam first reacts with CaO to form $Ca(OH)_2$ and then $Ca(OH)_2$ undergoes carbonation. The reaction formula is as follows:

$$CaO + H_2O \rightarrow Ca(OH)_2 \quad (6)$$

$$Ca(OH)_2 + 2CO_2 \leftrightarrow Ca(HCO_3)_2 \quad (7)$$

In this case, the rate of the carbonation reaction is catalyzed by H_2O by means of formation of transient $Ca(OH)_2$ which is more reactive than is CaO. However, the mechanism of the steam effect on carbonation reaction could not be distinguished based on our kinetic data.

The mechanism of the steam effect on decarbonation could be different. It was found that both steam and CO_2 molecules were adsorbed onto the $CaCO_3$ surface, with steam more strongly held, and able to displace CO_2 [43]. It has suggested that the adsorbed H_2O molecules weaken the bond between CaO and CO_2, and thus catalyze the decomposition of the crystal lattice.

4.4. Sorption enhanced reforming of methane (SESMR)

In SESMR, during the pre-breakthrough phase, three reactions: reforming, shift and carbonation are all active and the calcined $CaCeZrO_x$ is active to capture CO_2, and thereby the CO_2 concentration is low. At the same time, the reforming of methane reactions is driven toward completion by the CO_2 removal. The by-products of CO_2 and CO are minimized and the concentration of the H_2 attains at its maximum value. The duration of this period is a function of the acceptor properties (sorption capacity and sorption kinetics), its mass, and the operating conditions. The limitation of a single

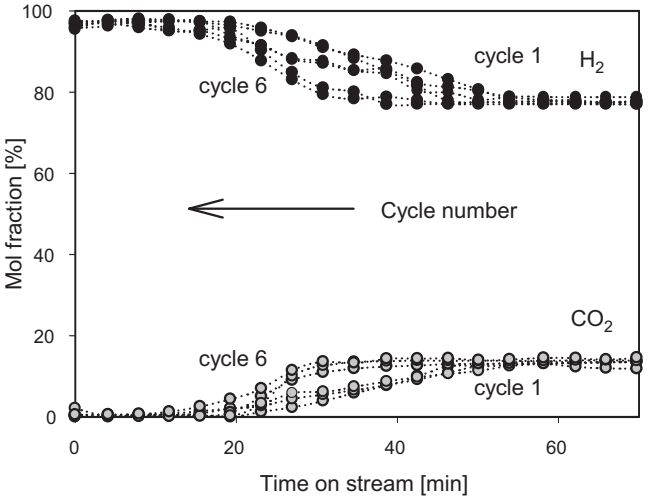

Fig. 9. Effluent H_2 and CO_2 concentration profiles on a water free basis. Acceptor: 5 g $CaCeZrO_x$, catalyst: 1 g 40 wt% NiHTlc. Acceptor/catalyst: 5, S/C: 3, F_{CH_4} = 45 cm^3/min, *T*: 843 K and *P*: 1 bar. Regeneration: *T*: 973 K, F_{Ar} = 100 cm^3/min.

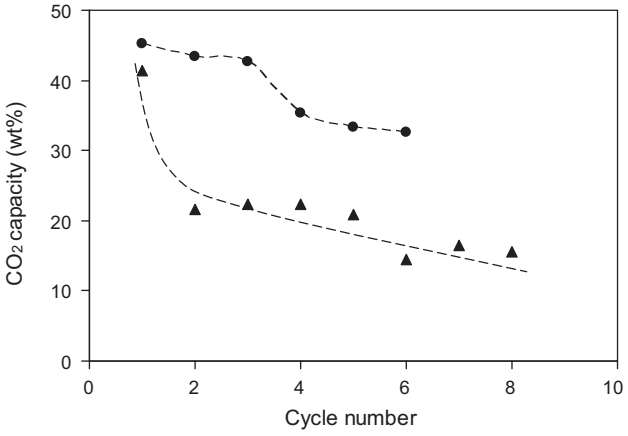

Fig. 10. CO_2 capture capacity of calcined CaCeZrOx through 6 cycles assessed in situ capture in steam methane reforming (●) and 8 cycles assessed in situ capture in the ethanol steam reforming (▲). In the case of in situ capture in steam methane reforming, decarbonation at 973 K in Ar and carbonation at 843 K. In the case of in situ capture of ethanol steam refoming, decarbonation at 1043 K in Ar and carbonation at 848 K.

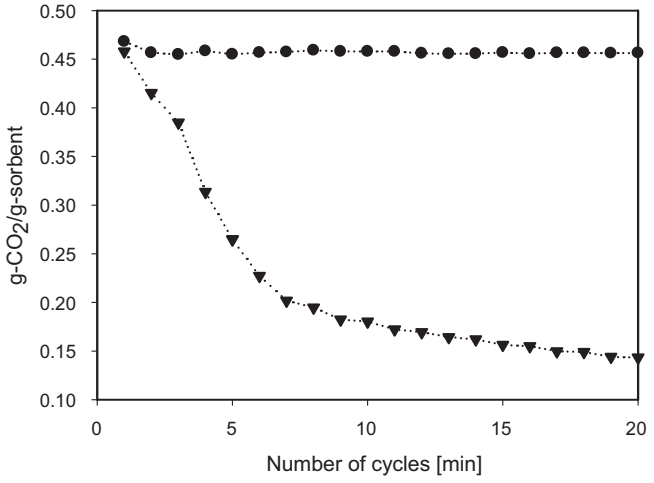

Fig. 11. CO_2 sorption capacities of the acceptor: (● $CaCeZrO_x$) and (▶ dolomite) respectively. Conditions: CaCeZr = 5.6 mg and dolomite = 5.5 mg. Temperature programmed range = 473–1173 K. Heating rate: 10 K/min, cooling rate: 50 K/min, carbonation: F_{CO_2}/F_{Ar} = 80 cm^3/min CO_2/20 cm^3/min Ar and decarbonation: F_{Ar} = 100 cm^3/min.

fixed bed is that continuous production of hydrogen is not possible. However, process economics requires that the acceptor should be regenerable and used in many reaction–regeneration cycles. In this perspective, two parallel fixed-bed reactors could be an alternative for continuous production of H_2 production and acceptor regeneration simultaneously, operated in a cyclic manner. Feed switchover time between two fixed-bed reactors is a critical value for achieving high performance in two parallel fixed bed reactors [44]. A fluidized-bed reactor with continuous carbonation in one reactor and decarbonation in another reactor is also a good alternative for continuous production of hydrogen [45].

During the experiments, after the acceptor bed had achieved the initial breakthrough, the bed was regenerated by decarbonation of the $CaCO_3$ formed in flowing N_2 at 973 K. This regeneration was performed in situ by heating the fixed bed containing acceptor–catalyst mixture concurrently. Subsequently, the catalyst–acceptor bed was subjected to a second SESMR-reaction cycle.

The effluent concentration profiles of both H_2 and CO_2 during successive cycles are presented in Fig. 9. The maximum H_2 concentration is effectively equal in the six cycles, although the duration of the pre-breakthrough is reduced somewhat as the number of cycles increased. Reduction in the prebreakthrough time indicates a decrease in the working capacity of the acceptor decreases with increasing number of cycle as shown in Fig. 10. There is a relatively large decrease in the capacity in the third cycle, and in the rest cycles the new acceptor seems to be relatively stable. However, a long term testing of acceptor stability at such realistic reaction conditions is needed in the future work.

The CO_2 capture capacity of the new $CaCeZrO_x$ acceptor obtained from SESMR is compared to the one of the dolomite obtained in sorption enhanced ethanol reforming [30] in Fig. 10. $CaCeZrO_x$ mixed oxide acceptor was used in SESMR whereas dolomite was used as an acceptor in SESR of ethanol. It is expected that the reaction of methane and ethanol reforming at similar conditions does not influence the capacity of the acceptors. The initial CO_2 capture capacity for both acceptors is more or less identical. However, Fig. 10 clearly indicates a much better stability of $CaCeZrO_x$ nanocrystals than the natural dolomite.

In order to get a better understanding of the difference in the two acceptors, the cyclic adsorption–desorption experiments were studied by temperature programmed carbonation (80 cm^3/min CO_2/20 cm^3/min Ar) and decarbonation (100 cm^3/min Ar) pressure of 0.8 bar and within the temperature range 473–1173 K. The results are presented in Fig. 11. It confirms the data obtained from SESMR that the $CaCeZrO_x$ nanocrystals are much more stable than the dolomites. Multiple cycles of carbonation–decarbonation reactions showed that $CaCeZrO_x$ mixed oxide acceptor attains a capture capacity of 0.456 g-CO_2/g-$CaCeZrO_x$ after 20 cycles. In contrast, natural dolomite shows poor performance with a capture capacity of 0.15 g-CO_2/g-dolomite after 20 cycles. $CaCeZrO_x$ is a superior acceptor compared to dolomite, with higher conversion of CaO (~94%) and better multi-cycle stability compared to dolomite, with low conversion of CaO (~33%) after 20 cycles. Dolomite gives only high conversion of CaO (~100%) in the first experimental cycle.

A comparison between Fig. 10 and Fig. 11 suggests that steam accelerated deactivation of CaO based CO_2 acceptors. It is in good agreement with reported results in literature [17,46,47], which has mostly been attributed to CaO sintering. Sintering of CaO occurs via solid-state ion diffusion [46,47], and steam obviously promotes solid-state ion diffusion. Again the steam effect on the stability is much smaller on the $CaCeZrO_x$ than on the dolomite. This could probably due to the inhibiting effect of well-dispersed inert

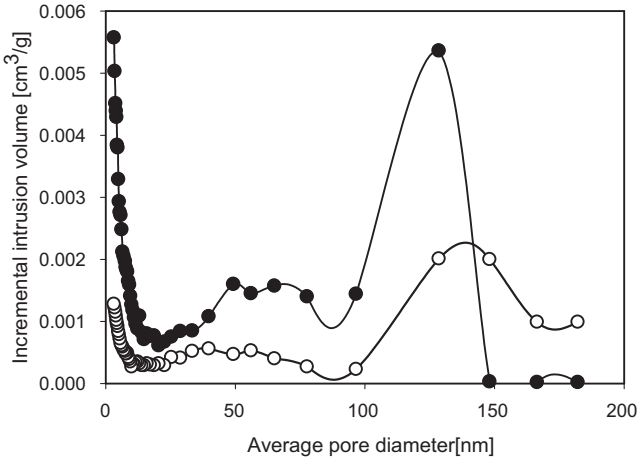

Fig. 12. Pore size distributions measured from N_2 physisorption (● $CaCeZrO_x$, ○ dolomite).

$Ce_{0.5}Zr_{0.5}O_2$ on ionic diffusion in the CaO or solid-state surface reaction between CaO particles.

It has been reported that the stability of the pore structure plays a significant role in the stability of the solid acceptors, since there is a significant volume change during the carbonation and decarbonation cycles [39]. Grasa and Abanades [36] and Sun et al. [48] have reported that limestone and dolomite, when subjected to a large number of cycles, lost completely the volume in small pores and give the uptake capacity lower than 0.1 g/g. Gupta and Fan [40] stated that the carbonation conversion of CaO samples from natural sources is very limited because of their microporous structure susceptible for pore filling and pore blockage, resulting from the formation of higher-volume product, $CaCO_3$. As a result capture capacity of dolomite deteriorates during multiple cycle operation [49,50].

The surface area and the pore volume of the $CaCeZrO_x$ and dolomite acceptors are listed in Table 1. By comparing the values in Table 1 and the pore size distribution in Fig. 12, a significant difference in the pore volume is observed between the two acceptors. The surface area of $CaCeZrO_x$ (31.1 m^2/g) and the pore volume (0.14 cm^3/g) are higher compared to dolomite surface area (8 m^2/g) and pore volume (0.04 cm^3/g) respectively. More importantly, the $CaCeZrO_x$ nanocrystals have a much large pore volumes in the pore size range between 10–100 nm and 100–150 nm than the dolomites.

The CO_2 capture capacity of dolomite decreases dramatically in the SESRE test in the first two cycles (Fig. 10), which is much faster than the decrease in the absence of the steam (Fig. 11). The $CaCeZrO_x$ nanocrystals are very stable in carbonation–decarbonation cycles at the dry conditions (Fig. 11), but it deactivates again in the real SESMR (Fig. 10). This can be ascribed an accelerated sintering of acceptors by steam. Therefore, the investigation of acceptors under dry conditions in TGA provides only a preliminary evaluation of the acceptor. It does not give any clue to their performance under real reforming conditions.

The reason for the fast deactivation of the dolomites can be two folds. At first, small pores in dolomites have a poor ability to tolerate the large volume changes of CaO particles inside the pores during the carbonation–decarbonation cycles. In addition, the backbone structure (MgO) in the dolomite is not stable enough, especially in the presence of the steam. As a result, the dolomites underwent the prompt closure of the pores throughout the particles and reduce the surface area of the CaO particles. Reduced porosity in the acceptor particles make it inaccessible to capture CO_2, leading to a fast decrease in the CO_2 uptake capacity in multicycling operation.

Table 3
The H_2 concentration and capture capacity of $CaCeZrO_x$ under different W/F_0.

W/F_0 [g/min/cm^3]	H_2 concentration [%]	Capture capacity [g-CO_2/g-$CaCeZrO_x$]
0.04	98	0.423
0.03	97	0.218
0.02	96	0.149

In our work, rapid decay of CO_2 capture capacity of CaO is solved by incorporating ceramic oxides in the CaO as the backbone structure and thus improved multicycle performance. The solid solution of refractory oxide formed between Ce–Zr provides a stable backbone structure and inhibiting sintering of the active CaO sites. The melting temperature of this refractory oxide is important because the diffusion of ions or atoms in a solid exponentially depends upon temperature. Vacancy diffusion in ionic compounds becomes significant only above about 3/4 of the absolute melting point. This is known as Tammann temperature. Solid materials start to sinter at or above their Tammann temperature, which is roughly about 50–75% of their bulk melting temperature. The reason for choosing zirconia and ceria as prospective refractory dopants in the present study is due to the fact that they exhibit relatively high Tammann temperatures (1491 K and 1337 K respectively). The backbone structure of the Ce–Zr mixed oxide in $CaCeZrO_x$ is expected to be much more stable than the MgO in dolomite. It could be also the important factor contribute to a better stability of CaO–Zr [14] and CaO–TiO_2 [15] mixed oxides. In addition, the nanoparticles of CaO reduced the local volume change in the pores during the carbonation and decarbonation cycles. The factors of large pores and CaO nanocrystals together with the stable backbone structure ($Ce_{0.5}Zr_{0.5}O_2$) make the new acceptor $CaCeZrO_x$ stable.

Another interesting observation is that a high CO_2 capacity was obtained at the SESMR conditions (Fig. 10), in spite of the low CO_2 gas phase concentration is expected in the SESMR reaction. The highest CO pressure in the reaction is 0.15 bar (Fig. 8) in the absence of the CO_2 removal. The CO_2 pressure is even lower (<0.03 bar, Fig. 8) in the gas phase with in situ CO_2 removal. Based on the relationship between CO_2 capacity and CO_2 pressure in Fig. 3, the maximum CO_2 capacity is about 20 wt% assuming in the gas phase reaching the equilibrium of the steam reforming and water gas shift reaction. In the real case the measured CO_2 concentration (Fig. 8) is much lower during the SESMR due to in situ CO_2 removal. In

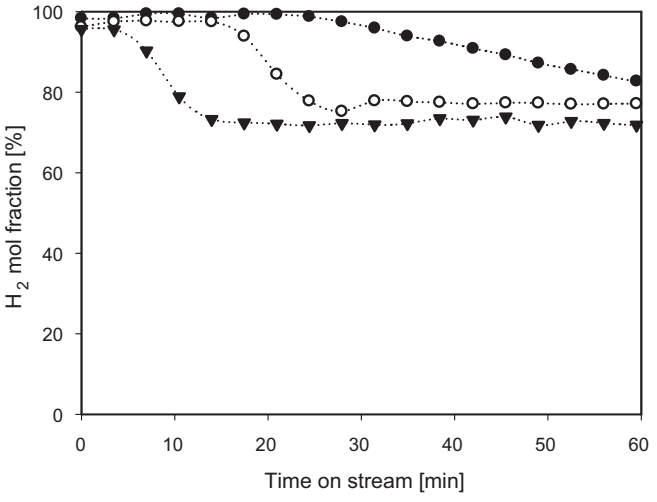

Fig. 13. Effluent H_2 concentration profiles on a water free basis. Acceptor: 10 g, catalyst: 40 wt% Ni-HTlc: 2 g. Acceptor/catalyst: 5, ● W/F_0 = 0.04, ○ W/F_0 = 0.03 and ▼ W/F_0 = 0.02 g/min/cm^3 respectively. T: 843 K.

this context, a much lower CO_2 capacity is expected. However, the measured CO_2 capacity is almost same as one at 0.8 bar CO_2 pressure measured in CO_2 capture kinetic study (Figs. 3 and 11). The very significant deviation in the CO_2 capacity measured in SESMR and CO_2 capture kinetic study strongly suggests a synergy effect between the catalytic reaction and CO_2 carbonation. The data here does not allow us to get an exclusive conclusion about the nature of the synergy effect. It will be an important topic for our future research.

Moreover, the effect of the residence time of methane has a significant effect on the CO_2 capture capacity. The experiments were carried out at following operation conditions: temperature of 843 K atmospheric pressure, steam/carbon mol ratio 3, and different weight of catalyst/feed (W/F_0) ratios. Table 3 indicates that longer residence time or higher the W/F_0, the higher the hydrogen yields. But the change is very small. As shown in Fig. 13, the time approaching to the breakthrough decreases with decreasing the residence time. It might be caused by a relatively large fraction of catalysts and acceptors under the low conversions. The results suggest an important principle in the design of SESMR process where the methane residence time could be more important for CO_2 capture than the hydrogen production. A kinetic study of CO_2 capture at SESMR conditions is necessary for SESMR reaction design.

5. Conclusions

A comparative kinetic study of CO_2 capture in both TGA and fixed bed reactor can be used for kinetic study in case sufficient high CO_2 flow is employed. TGA is still the simple method for screening the acceptors in terms of capacity and stability. Both TGA and the measurement of breakthrough curve in the fixed bed reactor provide almost identical CO_2 capacity, but the fixed bed reaction is a better tool for the kinetic study both for CO_2 capture and SESMR.

A new Ca-based CO_2 nanocrystalline acceptor, $CaCeZrO_x$ is synthesized by spray drying. This novel material gives high conversion and high cyclic CO_2 capture capacity during multicyclic carbonation–decarbonation. The enhanced performance can be attributed to stable backbone structure and the high surface area and large pore volume compared to dolomites. Previously studied results showed that high-purity of hydrogen can be obtained in sorption enhanced steam methane reforming using CaO, dolomite as CO_2 acceptors. However, a decrease in most multicylic studies limits sorption enhanced steam methane reforming. Our new $CaCeZrO_x$ mixed oxide acceptor produces 96% high purity of hydrogen at the low temperature of 843 K. Multicycle tests in situ capture in steam reforming of methane show a moderate decrease in the sorption capacity of $CaCeZrO_x$, providing incentive for further improvement and evaluation under steam reforming conditions.

We report a synergetic effect between the catalytic reaction and CO_2 carbonation by a comparative study between SESMR and CO_2 capture kinetics, which has not been reported previously. The capacity of the CO_2 capture on the acceptors in the SESMR cannot be simply predicted by independent CO_2 capture kinetic study. In addition, the residence time has a significant influence on the CO_2 capture. These two factors should be addressed in the future study in order to get a better understanding of the SESMR process.

Acknowledgement

The Norwegian Research Council (NFR) is acknowledged for financial support.

References

[1] D.P. Harrison, Ind. Eng. Chem. Res. 47 (2008) 6486.
[2] C. Han, D.P. Harrison, Chem. Eng. Sci. 49 (1994) 5875.
[3] J.R. Hufton, S. Mayorga, S. Sircar, AIChE J. 45 (1999) 248.
[4] E. Ochoa-Fernandez, G. Haugen, T. Zhao, M. Ronning, I. Aartun, B. Borresen, E. Rytter, M. Ronnekleiv, D. Chen, Green Chem. 9 (2007) 654.
[5] E. Ochoa-Fernández, M. Rønning, T. Grande, D. Chen, Chem. Mater. 18 (2006) 6037.
[6] T. Zhao, E. Ochoa-Fernández, M. Rønning, D. Chen, Chem. Mater. 19 (2007) 3294.
[7] S.F. Wu, Q.H. Li, J.N. Kim, K.B. Yi, Ind. Eng. Chem. Res. 47 (2007) 180.
[8] A. Silaban, D.P. Harrison, Chem. Eng. Commun. 137 (1995) 177.
[9] A.L. Ortiz, D.P. Harrison, Ind. Eng. Chem. Res. 40 (2001) 5102.
[10] A. Silaban, M. Narcida, D.P. Harrison, Chem. Eng. Commun. 146 (1996) 149.
[11] B. Balasubramanian, A.L. Ortiz, S. Kaytakoglu, D.P. Harrison, Chem. Eng. Sci. 54 (1999) 3543.
[12] K.B. Yi, D.P. Harrison, Ind. Eng. Chem. Res. 44 (2005) 1665.
[13] H. Lu, A. Khan, S.E. Pratsinis, P.G. Smirniotis, Energy Fuels 23 (2008) 1093.
[14] H. Lu, P.G. Smirniotis, F.O. Ernst, S.E. Pratsinis, Chem. Eng. Sci. 64 (2009) 1936.
[15] S.F. Wu, Y.Q. Zhu, Ind. Eng. Chem. Res. 49 (2010) 2701.
[16] Z.-S. Li, N.-S. Cai, Y.-Y. Huang, H.-J. Han, Energy Fuels 19 (2005) 1447.
[17] P. Sun, J.R. Grace, C.J. Lim, E.J. Anthony, Ind. Eng. Chem. Res. 47 (2008) 2024.
[18] V. Manovic, E.J. Anthony, Ind. Eng. Chem. Res. 49 (2010) 9105.
[19] F. Zeman, Int. J. Greenhouse Gas Control 2 (2008) 203.
[20] R.W. Hughes, D. Lu, E.J. Anthony, Y. Wu, Ind. Eng. Chem. Res. 43 (2004) 5529.
[21] S. Dobner, L. Sterns, R.A. Graff, A.M. Squires, Ind. Eng. Chem. Process Des. Dev. 16 (1977) 479.
[22] C. Han, A. Silaban, M. Narcida, D.P. Harrison, Technical report, DE95011399, Technical report to Department of Energy, US, 1994.
[23] D. Chen, A. Grønvold, H.P. Rebo, K. Moljord, A. Holmen, Appl. Catal. A 137 (1996) 1.
[24] D. Chen, E. Bjorgum, K.O. Christensen, A. Holmen, R. Lodeng, Adv. Catal. 51 (2007) 351.
[25] E. Ochoa-Fernández, T. Zhao, M. Rønning, D. Chen, J. Environ. Eng. 135 (2009) 397.
[26] D. Chen, A. Grønvold, H.P. Rebo, K. Moljord, A. Holmen, App. Catal. A: Gen. 137 (1996) 351.
[27] K.S. Sultana, S.A. Fagerbekk, L. He, T. Zhao, D. Chen, in preparation.
[28] E. Ochoa-Fernández, C. Lacalle-Vilà, K. Christensen, J. Walmsley, M. Rønning, A. Holmen, D. Chen, Top. Catal. 45 (2007) 3.
[29] L. He, H. Berntsen, E. Ochoa-Fernández, J. Walmsley, E. Blekkan, D. Chen, Top. Catal. 52 (2009) 206.
[30] L. He, H. Berntsen, D. Chen, J. Phys. Chem. A 114 (2010) 3834.
[31] R. Barker, J. Appl. Chem. Biotechnol. 23 (1973) 733.
[32] H. Lu, E.P. Reddy, P.G. Smirniotis, Ind. Eng. Chem. Res. 45 (2006) 3944.
[33] J.S. Dennis, R. Pacciani, Chem. Eng. Sci. 64 (2009) 2147.
[34] R. Pacciani, C.R. Müller, J.F. Davidson, J.S. Dennis, A.N. Hayhurst, Can. J. Chem. Eng. 86 (2008) 356.
[35] D. Alvarez, J.C. Abanades, Ind. Eng. Chem. Res. 44 (2005) 5608.
[36] G.S. Grasa, J.C. Abanades, Ind. Eng. Chem. Res. 45 (2006) 8846.
[37] A.I. Lysikov, A.N. Salanov, A.G. Okunev, Ind. Eng. Chem. Res. 46 (2007) 4633.
[38] C. Salvador, D. Lu, E.J. Anthony, J.C. Abanades, Chem. Eng. J. 96 (2003) 187.
[39] J. Blamey, E.J. Anthony, J. Wang, P.S. Fennell, Prog. Energy Combust. 36 (2010) 260.
[40] H. Gupta, L.-S. Fan, Ind. Eng. Chem. Res. 41 (2002) 4035.
[41] Z.-S. Li, N.-S. Cai, Energy Fuels 21 (2007) 2909.
[42] S.F. Wu, T.H. Beum, J.I. Yang, J.N. Kim, Ind. Eng. Chem. Res. 46 (2007) 7896.
[43] Y. Wang, W.J. Thomson, Chem. Eng. Sci. 50 (1995) 1373.
[44] Z.-S. Li, N.-S. Cai, J.-B. Yang, Ind. Eng. Chem. Res. 45 (2006) 8788.
[45] Z. Chen, J.R. Grace, C.J. Lim, Ind. Eng. Chem. Res. (2011), doi:10.1021/ie101360x.
[46] R.H. Borgwardt, Ind. Eng. Chem. Res. 28 (1989) 493.
[47] R.H. Borgwardt, Chem. Eng. Sci. 44 (1989) 53.
[48] P. Sun, J.R. Grace, C.J. Lim, E.J. Anthony, AIChE J. 53 (2007) 2432.
[49] D. Alvarez, J.C. Abanades, Energy Fuels 19 (2004) 270.
[50] K.O. Albrecht, K.S. Wagenbach, J.A. Satrio, B.H. Shanks, T.D. Wheelock, Ind. Eng. Chem. Res. 47 (2008) 7841.